Block-based Compressive Low-light-level Imaging

Jun Ke*, Ping Wei*, Xin Zhang† and Edmund Y. Lam‡
*Key Laboratory of Photo-electronic Imaging Technology and System, Ministry of Education of China,
School of Optoelectronics, Beijing Institute of Technology, Beijing, China
†National Laboratory of Pattern Recognition, Institute of Automation, Chinese Academy of Sciences, Beijing, China
‡Electrical and Electronic Engineering Department, University of Hong Kong, Pokfulam, Hong Kong, China

***Abstract*—In this paper, block-based compressive low-light-level imaging (BCL-imaging) is studied. To obtain larger measurement SNR (signal to noise ratio), instead of object pixels, linear combinations of pixels, referred to as features, are collected. PCA and Hadamard features are studied. Measurement SNR and reconstruction error are analyzed to quantify BCL-imaging performance. Compared with conventional imaging, BCL-imaging presents better reconstruction quality. Between PCA and Hadamard projections, PCA has smaller reconstruction error. However, after sorting the projection vectors using measurement SNR, Hadamard can obtain similarly performance as PCA. Biased vector and dual-measurements are studied with experimental results for the implementation of both projections in the end of this paper.**

I. Introduction

Low-light-level imaging (L^3-imaging) has broad applications such as night vision, under water imaging, life science, and astronomy [1]–[4]. In L^3-imaging, an object is focused onto the photocathode of an image intensifier. Then the received signal power is magnified using high voltage to accelerate electrons and create multiple time re-emissions. Because L^3-imaging is used for weak light signals, its essential issue is to increase system magnification or measurement SNR (signal to noise ratio) values. To have a large magnification, through last couple of decades 4 generation intensifiers have been studied [5], [6]. In this work, a new method named as block-based compressive low-light-level imaging (BCL-imaging) is studied to further improve system measurement SNR [7]–[11].

II. Block-based Compressive Low-light-level Imaging (BCL-imaging)

Figure 1(a) presents a BCL-imaging system diagram. In such a system, an object is focused and spatially modulated by a DMD (digital micromirror device). Then the modulated signal is refocused onto the intensifier for magnification. After the intensifier, a detector array is used to measure the amplified signal. Then reconstruction algorithm is used to estimate the object from the measurements.

The part before the intensifier in BCL-imaging is similar to a block-based compressive imaging (BCI) system as shown in Figure 1(b) [7], [12]. Using BCI architecture in L^3-imaging is to enlarge the received signal power at the photocathode. In BCI, the spatial light modulation process is implemented based on object blocks. For example, an $(\sqrt{NK} \times \sqrt{NK})$ object has K blocks of size $(\sqrt{N} \times \sqrt{N})$. Each block is spatially modulated, then focused onto one detector for measurements. Modifying the patterns displayed on DMD, then multiple measurements for each block, referred to as features, can be obtained [13]. Collecting object features instead of pixels can improve measurement SNR [13], [14]. Therefore, in this work, a BCI part is used on top of an image intensifier for low-light-level imaging.

The measurement process in BCL-imaging can be represented as following,

$$\mathbf{Y} = p\mathbf{F}\mathbf{X} + \mathbf{N}, \tag{1}$$

where p is the magnification of an intensifier, $\mathbf{F} = [\ \mathbf{f}_1 \quad \mathbf{f}_2 \quad \cdots \quad \mathbf{f}_M\ ]^{\mathrm{T}}$ is the projection matrix with each row as a projection vector. PCA (principal component analysis) and Hadamard projections are analyzed in this work. Matrixes $\mathbf{Y}$, $\mathbf{X}$, and $\mathbf{N}$ are the measurement, object, and noise matrixes, respectively. Each column of these matrixes is for one object block. The detector noise in each measurement is assumed to be an independent white Gaussian noise with variance σ^2.

To reconstruct objects, we define the object autocorrelation matrix as $\mathbf{R}_{\mathbf{x}} = E\left\{\|\mathbf{x}\mathbf{x}^{\mathrm{T}}\|^2\right\} = \mathbf{Q}\mathbf{D}\mathbf{Q}^{\mathrm{T}}$, where $\mathbf{x}$ is the vector for one object block, $\mathbf{Q}$ is equal to $[\ \mathbf{q}_1 \quad \mathbf{q}_2 \quad \cdots \quad \mathbf{q}_N\ ]$ with $\mathbf{Q}\mathbf{Q}^{\mathrm{T}} = \mathbf{I}$ and matrix $\mathbf{D}$ is a diagonal matrix with diagonal elements $\{d_1, d_2, \cdots, d_N\}$. These elements are the eigenvalues of $\mathbf{R}_{\mathbf{x}}$, while $\mathbf{q}_i$ is the eigenvector corresponding to the eigenvalue d_i. Using these definitions, the reconstruction Wiener operator for BCL-imaging is defined as

$$\mathbf{W} = p\mathbf{R}_{\mathbf{x}}\mathbf{F}^{\mathrm{T}}\left(p^2\mathbf{F}\mathbf{R}_{\mathbf{x}}\mathbf{F}^{\mathrm{T}} + \sigma^2\mathbf{I}\right)^{-1}. \tag{2}$$

Then an object can be estimated from its feature measurements as $\mathbf{X}_{\text{est}} = \mathbf{W}\mathbf{Y}$.

To analyze BCL-imaging system performance, pixel-wised measurement SNR and system reconstruction error, normalized RMSE (root mean square error), can be calculated using Equation 3 and 4 [15]

$$\begin{aligned} SNR_{\text{CS}} &= \frac{E\{\|p\mathbf{F}\mathbf{X}\|^2\}}{E\{\|\mathbf{N}\|^2\}} \\ &= \frac{\mathrm{Tr}\{p^2\mathbf{F}\mathbf{R}_{\mathbf{x}}\mathbf{F}^{\mathrm{T}}\}}{M\sigma^2}, \end{aligned} \tag{3}$$

$$\begin{aligned} RMSE_{\text{CS}} &= \sqrt{\frac{E\{\|\mathbf{X}_{\text{est}} - \mathbf{X}\|^2\}}{E\{\|\mathbf{X}\|^2\}}} \\ &= \sqrt{\frac{\mathrm{Tr}\{\mathbf{R}_{\mathbf{x}} - p^2\mathbf{F}\mathbf{R}_{\mathbf{x}}^{\mathbf{2}}\mathbf{F}^{\mathrm{T}}(p^2\mathbf{F}\mathbf{R}_{\mathbf{x}}\mathbf{F}^{\mathrm{T}} + \sigma^2\mathbf{I})^{-1}\}}{\mathrm{Tr}\{\mathbf{R}_{\mathbf{x}}\}}}. \end{aligned} \tag{4}$$

978-1-4673-5791-3/13/$31.00 ©2013 IEEE

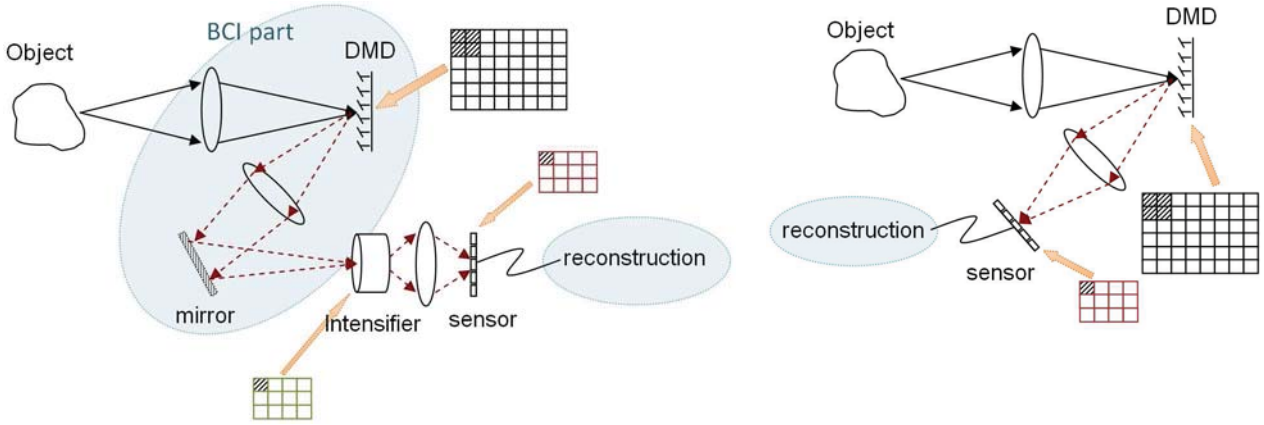

(a) (b)

Fig. 1. (a) A BCL-imaging system diagram; (b) A BCI system diagram.

As a comparison, conventional L^3-imaging is also studied in this work. To make the comparison fair, M measurements are collected in the conventional system, because M features for each object block in BCL-imaging are collected. The final measurement result for a conventional system is the average of these M measurements. Same as in BCL-imaging, the detector noise in each measurement is assumed to be a Gaussian noise $N(0, \sigma^2)$. The measurement SNR and the normalized reconstruction RMSE for conventional low light imaging can be represented as

$$SNR_{\text{conv}} = \frac{\text{Tr}\{p^2 \mathbf{R_x}\}}{N\sigma^2/M}, \tag{5}$$

$$RMSE_{\text{conv}} = \sigma / \sqrt{M \text{Tr}\{\mathbf{R_x}\}}, \tag{6}$$

III. Experimental Results

The first experiment is to observe the variation of reconstruction error in BCL-imaging as a function of the number of feature measurements M. In this experiment, PCA features are collected for an (2610×4000) object. The PCA vectors, or the eigenvectors $\mathbf{q}_i$ of $\mathbf{R_x}$, are sorted based on its eigenvalues d_i. It means a vector $\mathbf{q}_i$ corresponding to a larger eigenvalue d_i is used to collect feature measurement first. The block size is set to be 32×32. Figure 2 presents the numerical evaluated RMSE vs. M for noise $\sigma = 10$, 45.8, 64.0, and 148.7 respectively. From Figure 2, the RMSE reduces as M increases for each noise level. However, when M is large enough, more feature measurements do not improve the reconstruction quality, because more noise is also collected into the measurements.

Using the same object, Figure 3(a) presents the measurement SNR obtained in a conventional L^3-imaging and a BCL-imaging. PCA projection is still used in the experiment. The number of measurements in both systems, M, are set to be 4, 8, and 12. From Figure 3(a), it can be observed that for all M values, BCL-imaging has larger SNR values. However, as M increase, the measurement SNR for a conventional system is increased as expected, while it is decreased for BCL-imaging.

In Figure 3 (b), the normalized RMSE values for both systems are plotted as a function of the detector noise standard deviation σ. For all noise levels BCL-imaging has smaller reconstruction error. The RMSE difference between the two imaging systems increases fast as σ increases. The reconstructions using conventional low-light-level imaging and BCL-imaging for $M = 4$ and $\sigma = 46$ are presented in Figure 3(c) and (d), respectively. Visually, the reconstruction using BCL-imaging has much better quality. Figure 4 presents another reconstruction example with $M = 4$ for the same noise level. Once again, smaller RMSE value is obtained using BCL-imaging.

In Figure 5, the measurement SNR and reconstruction RMSE values for the conventional and the BCL-imaging using Hadamard projection are presented. The elements in the projection matrix is normalized to -1 and $+1$. In this experiment, the Hadamard vectors are sorted based on the variation in a vector. It means the low frequency component in an object block is collected first as a measurement. Comparing Figure 5 and 3, the RMSE value for Hadamard projection is larger than the PCA projection. To improve the system performance with Hadamard, measurement SNR is used to sort the vectors.

Using $\mathbf{f}_i$ and $\mathbf{q}_i$ to rewrite the measurement SNR in Equation 3, we have

$$\begin{aligned} SNR_{\text{CS}} &\propto \text{Tr}\{\mathbf{F}\mathbf{R_x}\mathbf{F}^{\text{T}}\} \\ &\propto \sum_{j=1}^{M} \left(\sum_{i=1}^{N} d_i (\mathbf{f}_j^{\text{T}} \mathbf{q}_i)^2 \right). \end{aligned} \tag{7}$$

From Equation 7, it is clear that the contribution of each projection vector to the measurement SNR, $\left\{ \sum_{i=1}^{N} d_i (\mathbf{f}_j^{\text{T}} \mathbf{q}_i)^2, j = 1, 2, \cdots, M \right\}$, is independent to each other. Therefore, we can calculate $\sum_{i=1}^{N} d_i (\mathbf{f}_j^{\text{T}} \mathbf{q}_i)^2$ for each $\mathbf{f}_j$ separately, and then use this value to sort $\{\mathbf{f}_j\}$. Figure 6 presents the RMSE in BCL-imaging using Hadamard projections sorted based on vector variation and measurement SNR. The results using PCA are also presented for comparison. Figure (a) is for the first object, while (b) is for the second. It can be observed that the new sorting criteria can improve the performance of the BCL-imaging system using Hadamard projection. The obtained RMSE values are

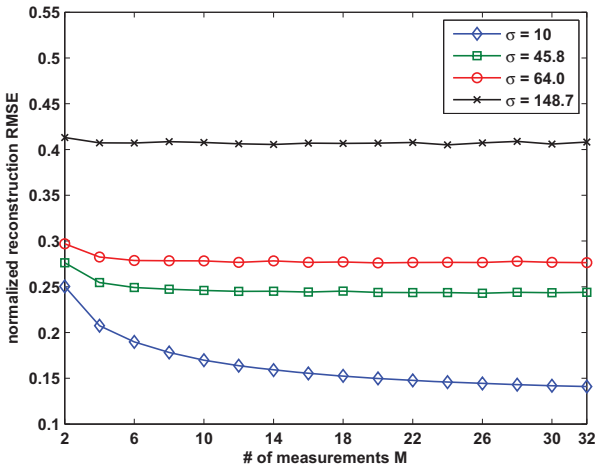

Fig. 2. RMSE vs. M for different noise level $\sigma = 10$, 45.8, 64, and 148.7, while the object has size 2610×4000 with block size 32×32.

very close to the values obtained using PCA, while it is much easier to implement the binary Hadamard vectors compared with PCA.

In the last experiment, we considered several practical conditions for BCL-imaging. First, because feature measurements are collected sequentially, each projection vector can be normalized by its maximal absolute element to enlarge the collected object signal. Second, PCA projection has positive and negative element values. Therefore, measurements for the positive part and the negative part can be collected separately, then combined together to obtain the final measurements. This is the dual-measurement method. In this method, two times noise are collected in the features due to the doubled measurements for one feature. Note that the feature collection time is also doubled. Another method to collect PCA features is to subtract each projection vector with its minimum element. Then the vector becomes non-negative. We referred this method as the biased-projection method. Similarly, Hadamard projection also has positive and negative elements, $\{-1, +1\}$. For this projection, we only consider to shift the vectors' dynamic range to non-negative region. One way is to sort the vectors using Equation 7 first. Then we plus those vectors with 1 followed by a normalization. Another way is to shift the element dynamic range from $[-1, 1]$ to $[0, 1]$, then sort the resulting vectors using Equation 7. In either case, Hadamard vectors with elements $\{0, 1\}$ are used for feature collection.

Figure. 7 (a) presents the RMSE vs. noise σ using PCA projection. The dual-measurement and the biased-projection methods are used, while the original PCA results are also presented for comparison. In the Figure, it is clear that normalizing the projection vectors improves BCL-imaging system performance much, especially for very high noise level. If we compare the results for same number of features, for example, for $M = 2$ or 12, the dual-measurement method presents smaller RMSE. However, if the number of measurements is fixed, the biased-projection has better performance. For example, for $M = 2$ features, the dual-measurement method needs 4 measurements for reconstruction. Compared this result, the green dash line with square marker, with the biased-projection method when $M = 4$, the red dot line with circle marker, the latter has smaller error values.

In Figure. 7 (b), we compared two biased Hadamard projection methods, one labeled as H_{dual}, in which the original Hadamard vectors are sorted first then followed by the bias process, the other labeled as H_{bias} for the case that the bias process is implemented first. The result using the originally SNR sorted projection, in which $\mathbf{F}$ has elements, $\{-1, 1\}$, is also shown in the figure. From the figure, the modification of the dynamic range of $\mathbf{F}$ significantly improves BCL-imaging performance. Between H_{dual} and H_{bias} cases, when $M = 2$, the two methods have no difference. This is due to same Hadamard vectors are used in both methods. However, for $M = 12$, the H_{dual} case presents smaller RMSE value. This means the orthogonality among the vectors plays an important role for the vector sorting process.

In the end, from Figure. 7 (a) and (b), it can be observed that the Hadamard projection presents comparable RMSE performance as PCA. Because Hadamard is a binary projection, its implementation is easier. In addition, because DMD device using time division for gray value display, it makes the measurement collection time for PCA vector is longer than Hadamard. Therefore, the feature collection for PCA needs longer time.

IV. Conclusion

In this work, a block-based compressive imaging architecture is used for low-light-level imaging. PCA and Hadamard features are collected for object reconstruction. For both kinds of features, the compressive imaging method presents better measurement SNR and reconstruction performance, especially for high noise level. Compared to PCA projection, Hadamard project's performance is worse. However, the difference between these two kinds of projections can be significantly reduced using the measurement SNR sorting method.

The work is supported by Key Laboratory of Photoelectronic Imaging Technology and System, Beijing Institute of Technology, Ministry of Education of China, under project 2013OEIOF02 and Beijing Institute of Technology Basic Research Fund under project 20120442006.

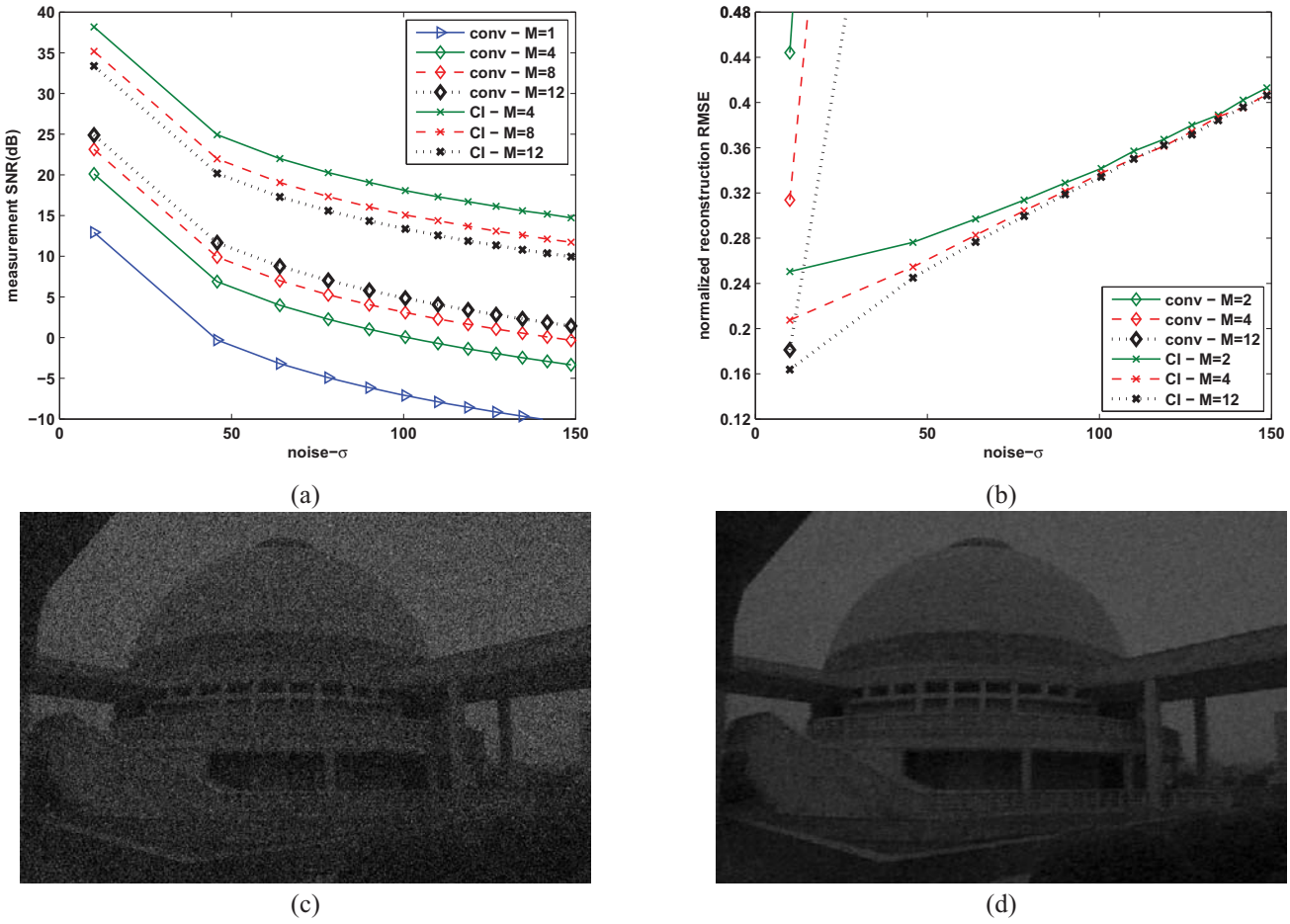

Fig. 3. (a) Measurement SNR(dB) vs. noise σ; (b) normalized RMSE vs. noise σ; (c) reconstruction in conventional L^3-imaging using 4 measurements with $\sigma = 46$; (d) reconstruction in BCL-imaging using 4 PCA features with $\sigma = 46$, while the object has size 2610×4000 with block size 32×32.

REFERENCES

[1] E.A. Richards. Limitations in optical imaging devices at low light levels. *Applied Optics*, 8(10):1999–2005, October 1969.

[2] R.E. Ansorge C.E. Hooper and J.G. Rushbrook. Low-light imaging technology in the life sciences. *Journal Biolumin Chemilumin*, 9:113–122, October 1994.

[3] Takashi Noji. X ray image intensifier, August 1987. US Patent 4,686,417.

[4] J. Anthony Tyson. Low-light-level charge-coupled device imaging in astronomy. *J. Opt. Soc. Am. A*, 3(12):2131–2138, December 1986.

[5] Ting-Zhu Bai and Wei-Qi Jin. *Optoelectronic Imaing Theory and Technology*. Beijing Institute of Technology Press China, 2010.

[6] Yue-Song Jiang. *Optoelectronics Technology and Experiment*. Beijing Institute of Technology Press China, 2000.

[7] Jun Ke and Edmund Y. Lam. Object reconstruction in block-based compressive imaging. *Optics Express*, 20(20):22102–22117, September 2012.

[8] Emmanuel J. Candès. Compressive sampling. In *Proceedings of the International Congress of Mathematicians*, volume 3, pages 1433–1452. European Mathematical Society, 2006.

[9] David L Donoho. Compressed sensing. *IEEE Transactions on Information Theory*, 52(4):1289–1306, April 2006.

[10] Dharmpal Takhar, Jason N. Laska, Michael B. Wakin, Marco F. Duarte, Dror Baron, Shriram Sarvotham, Kevin F. Kelly, and Richard G. Baraniuk. A new compressive imaging camera architecture using optical-domain compression. *IS&T/SPIE Computational Imaging IV*, 6065:606509(1)–606509(10), January 2006.

[11] Marco F. Duarte, Mark A. Davenport, Dharmphal Takhar, Jason N. Laska, Ting Sun, Kevin F. Kelly, and Richard G. Baraniuk. Single-pixel imaging via compressive sampling. *IEEE Signal Processing Magazine*, 25(2):83–91, March 2008.

[12] Jun Ke and Edmund Y. Lam. Nonlinear image reconstruction in block-based compressive imaging. In *IEEE International Symposium on Circuits and Systems*. IEEE, 2012.

[13] Mark A. Neifeld and Jun Ke. Optical architectures for compressive imaging. *Applied Optics*, 46(22):5293–5303, July 2007.

[14] Mark A. Neifeld and Premchandra Shankar. Feature-specific imaging. *Applied Optics*, 42(17):3379–3389, June 2003.

[15] Jun Ke, Michael D. Stenner, and Mark A. Neifeld. Minimum reconstruction error in feature-specific imaging. In *Proceedings of SPIE*, volume 5817, pages 7–12. SPIE, 2005.

(a) (b)

Fig. 4. (a) Reconstruction in conventional L^3-imaging using 4 measurements with $\sigma = 46$; (b) reconstruction in BCL-imaging using 4 PCA features with $\sigma = 46$, while the object has size 3000×4000 with block size 32×32.

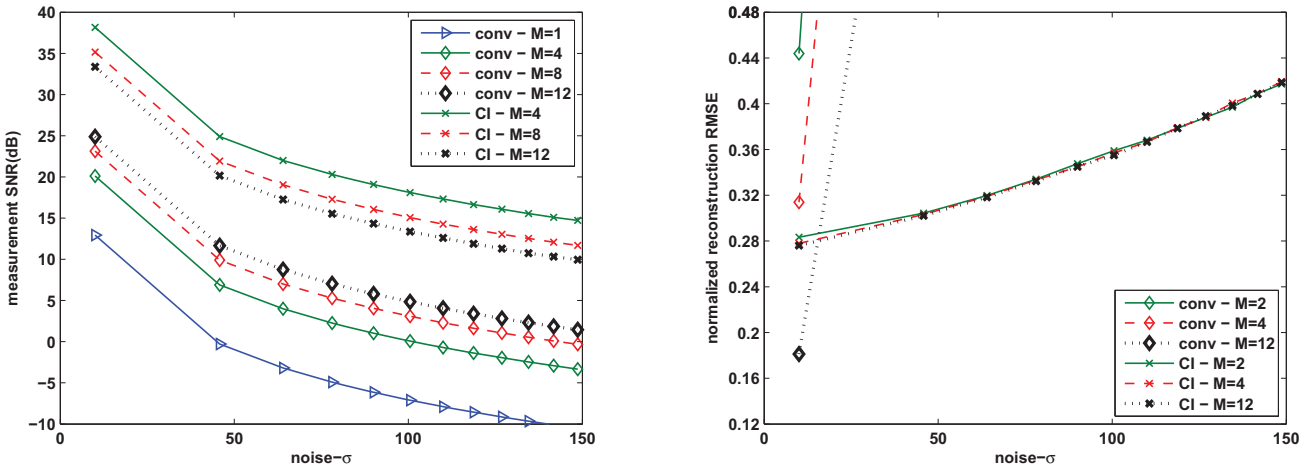

(a) (b)

Fig. 5. (a) Measurement SNR(dB) vs. noise σ; (b) normalized RMSE vs. noise σ, while Hadamard features are collected for the object of size 2610×4000 with block size 32×32.

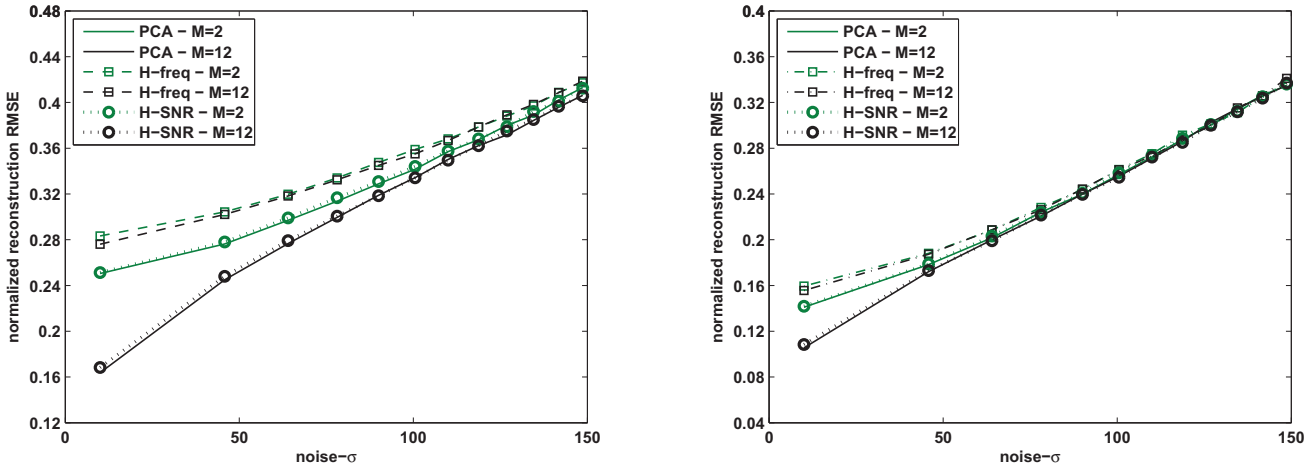

(a) (b)

Fig. 6. Normalized RMSE vs. noise σ for Hadamard sorted using different methods. The object has size (a) 2610×4000 and (b) 3000×4000 with block size 32×32. Result using PCA features are presented for comparison.

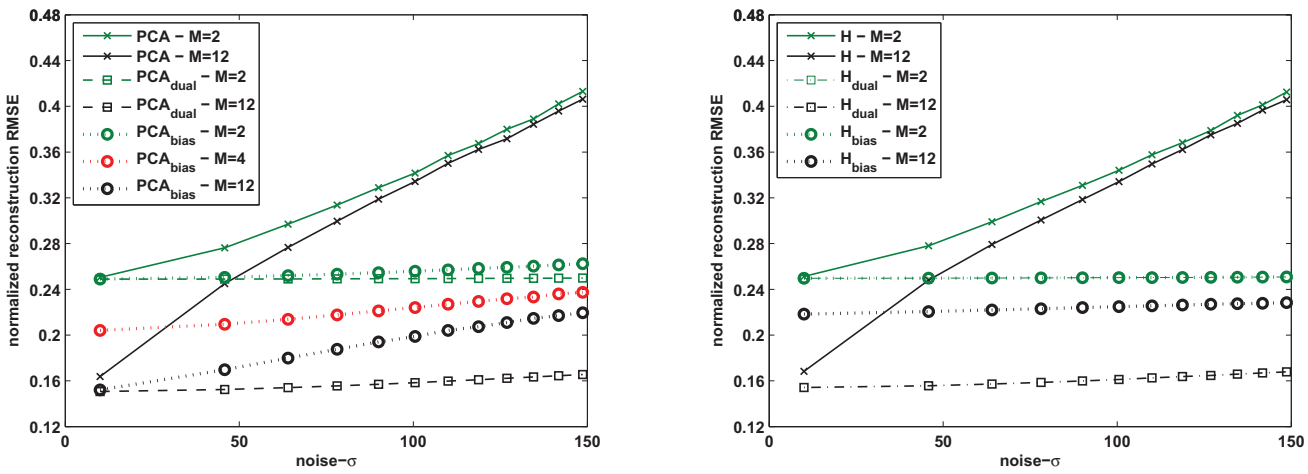

(a) (b)

Fig. 7. Normalized RMSE vs. noise σ for practical implemented (a) PCA and (b) Hadamard projection for the object of size 2610×4000 with block size 32×32.